Strong shock waves and nonequilibrium response in a one-dimensional gas: A Boltzmann equation approach

Pablo I. Hurtado
Department of Physics, Boston University, Boston, Massachusetts 02215, USA
and Institute Carlos I for Theoretical and Computational Physics, Universidad de Granada, 18071 Granada, Spain
(Received 2 May 2005; published 17 October 2005)

We investigate the nonequilibrium behavior of a one-dimensional binary fluid on the basis of Boltzmann equation, using an infinitely strong shock wave as probe. Density, velocity, and temperature profiles are obtained as a function of the mixture mass ratio μ. We show that temperature overshoots near the shock layer, and that heavy particles are denser, slower, and cooler than light particles in the strong nonequilibrium region around the shock. The shock width $\omega(\mu)$, which characterizes the size of this region, decreases as $\omega(\mu) \sim \mu^{1/3}$ for $\mu \to 0$. In this limit, two very different length scales control the fluid structure, with heavy particles equilibrating much faster than light ones. Hydrodynamic fields relax exponentially toward equilibrium: $\phi(x) \sim \exp[-x/\lambda]$. The scale separation is also apparent here, with two typical scales, λ_1 and λ_2, such that $\lambda_1 \sim \mu^{1/2}$ as $\mu \to 0$, while λ_2, which is the slow scale controlling the fluid's asymptotic relaxation, increases to a constant value in this limit. These results are discussed in light of recent numerical studies on the nonequilibrium behavior of similar one-dimensional binary fluids.

DOI: 10.1103/PhysRevE.72.041101 PACS number(s): 05.20.Dd, 05.20.Jj, 47.70.Nd, 05.70.Ln

I. INTRODUCTION

When a piston moves at constant velocity into a fluid, it generates a shock wave [1]. This is a strong perturbation that drives the system far from equilibrium. Studying the structural properties of the shock wave, and how equilibrium is restored behind it, we may extract valuable information on the fluid's transport properties, the damping of nonequilibrium fluctuations, etc. That is, we may use the shock wave as a probe to better understand the nonequilibrium response of the fluid. This is particularly appealing for one-dimensional (1D) systems. Their nonequilibrium behavior has attracted much attention during the last years [2–19]. This follows from two main reasons. On one hand, the dimensional constraint characteristic of 1D systems plays an essential role in many real structures, ranging from carbon nanotubes [4] to anisotropic crystals [5], magnetic systems [6], solid copolymers [7], semiconductor wires [8], zeolites [9], Bose-Einstein condensates [10], colloids in narrow channels [11], DNA, nanofluids, etc [2]. On the other hand, the simplicity and versatility of 1D models allow one to tackle fundamental questions in nonequilibrium statistical mechanics, such as those related to irreversibility, normal transport, equipartition, local thermodynamic equilibrium, etc. [2].

In this way, it has been found that the low dimensionality can give rise to anomalous transport properties in 1D fluids. To be more specific, the *single-file* constraint characteristic of 1D fluids introduces strong correlations between neighboring particles, which asymptotically suppress mass transport [11] and enhance heat conduction [12–19]. In particular, it is currently believed (see, however, [12,13]) that 1D fluids with momentum-conserving interactions and nonzero total pressure exhibit a thermal conductivity κ that diverges as $\kappa \sim L^{\gamma}$ when the system size $L \to \infty$ [14–18]. However, there is no complete agreement yet on the exponent $\gamma > 0$: there exists strong numerical and theoretical evidence pointing out that $\gamma = 1/3$ [14,15], although mode-coupling theories and Boltzmann equation analysis predict $\gamma = 2/5$ [16,17], while other numerical results are closer to $\gamma = 1/4$ [18]. Conservation of momentum seems to be crucial; as soon as this symmetry is broken, normal heat transport is recovered [19]. Moreover, momentum-conserving 1D fluids typically exhibit other anomalies when perturbed away from equilibrium, as, for instance, dynamic nonequipartition of energy, emergence of multiple relaxation scales, energy localization, etc. [12,13,15,18,20]. In general, the behavior of 1D fluids far from equilibrium still poses many intriguing questions that require further investigation.

In this paper we probe the nonequilibrium response of a 1D model gas. In particular, we address the problem of an *infinitely strong* shock wave propagating into a 1D binary fluid, within the context of the Boltzmann equation [21–23]. The shock wave characterizes the transition between two different asymptotic equilibrium states of the fluid. For strong shock waves (to be specified later), this transition happens within molecular scales, so that kinetic (Boltzmann) equations must be used. In fact, one may think of the shock wave problem as the simplest case study dominated by the nonlinearity of the Boltzmann equation [26]. As we will see below, the Boltzmann equation provides a powerful tool to investigate the observed structural and relaxational anomalies in 1D fluids. Kinetic theory methods have been applied to study strong shock waves in high-dimensional *simple* fluids [24–26]. However, in one dimension, a simple (i.e., monocomponent) fluid constitutes a pathological limit [27]. This follows from the fact that particles with equal masses in 1D interchange their velocities upon collision, so that a 1D monocomponent fluid can be regarded to a large extent as an ideal gas of noninteracting particles [28]. We may restore ergodicity and relaxation in velocity space by introducing different masses. The simplest case is that of a binary mixture. In particular, we study in this paper a binary 1D fluid composed by two species of hard-point particles, with masses $m_1 < m_2$ and *equal* concentrations. Energy transport in this model has already been extensively studied via molecular dynamics simulations [12,13,15,18,37].

The structure of the paper is as follows. In Sec. II, we write down the relevant Boltzmann equation for our 1D binary fluid, and extend a method by H. Grad [24,26] to study the structure of an infinitely strong shock wave propagating through the fluid. The results of this approach are described in Sec. III. In particular, we study there the shock hydrodynamic profiles, paying special attention to the shock width and the relaxation toward equilibrium, as a function of the mass ratio. Finally, in Sec. IV we discuss our results.

II. THE SHOCK-WAVE PROBLEM

The Boltzmann equation for a 1D binary fluid in a reference frame moving with the shock wave reads [21–23,26,29]

$$v\frac{df_1}{dx} = \mathcal{Q}_1(f_1,f_2) - f_1\nu(f_2), \tag{1}$$

$$v\frac{df_2}{dx} = \mathcal{Q}_2(f_2,f_1) - f_2\nu(f_1). \tag{2}$$

Here, $f_i(x,v)$ is the probability density for finding a particle of type $i=1,2$ (i.e., mass m_i) at position x with velocity v, and $\mathcal{Q}_i$ and ν represent the gain term and collision frequency in the collision operator, respectively. They are defined as

$$\mathcal{Q}_i(f_i,f_j) = \int_{-\infty}^{+\infty} dw|v-w|f_i(x,v_i')f_j(x,w_i'), \tag{3}$$

$$\nu(f_i) = \int_{-\infty}^{+\infty} dw|v-w|f_i(x,w). \tag{4}$$

Index j refers here to particle species other than i, and (v_i', w_i') are precollisional velocities that after collision give rise to velocities (v,w) for the pair (i,j); namely,

$$v_i'(v,w) = \frac{(m_i-m_j)v + 2m_j w}{m_i+m_j},$$

$$w_i'(v,w) = \frac{(m_j-m_i)w + 2m_i v}{m_i+m_j}. \tag{5}$$

Notice that Eqs. (1) and (2) only include the effect of cross-collisions between the different species, and no self-collisions between like particles. This reflects the one-dimensional character of our model fluid, and it is a main contrast to the Boltzmann equation for mixtures in higher dimensions.

The structure of the shock wave can be deduced from Eqs. (1) and (2) subject to the boundary conditions

$$f_i(x,v) \to G_{i,\pm}(v), \quad \text{as} \quad x \to \pm\infty, \tag{6}$$

where

$$G_{i,\pm}(v) \equiv n_\pm \sqrt{\frac{m_i}{2\pi T_\pm}} \exp\left[-\frac{m_i(v-u_\pm)^2}{2T_\pm}\right]. \tag{7}$$

Here $n_\pm$, $T_\pm$, and $u_\pm$ are, respectively, the number density, temperature, and macroscopic velocity at $x\to\pm\infty$ [30]. One usually chooses $u_+>0$, which implies (see below) $u_->0$. This represents a flow of the fluid mixture from $-\infty$ (upstream or preshock region) to $+\infty$ (downstream or aftershock region).

We are particularly interested in the structure of an *infinitely strong* shock wave. In this way we can probe the response of the 1D binary mixture in the strong nonequilibrium regime, far from the linear response region [22]. The strength of a shock may be defined in several ways. One of them is based on the ratio of downstream to upstream pressures, $r=p_+/p_-$, where $p_\pm=n_\pm T_\pm$. Weak shocks have a ratio r close to unity. In this case, the shock thickness is large as compared to the mean free path, and continuum approximations of the type of Navier-Stokes (or Euler, Burnett, etc.) may be used to characterize the shock structure [1]. However, as r grows the shock thickness becomes comparable to the mean free path, making inappropriate the application of hydrodynamic approximations. In this case kinetic equations, as those in (1) and (2), must be used instead. We pay attention in what follows to the limit $r\to\infty$, or equivalently, $T_-\to 0$.

The parameters entering the two limiting Maxwellians (7) are related due to conservation of particle number, total momentum, and total energy. Such conservation laws can be expressed as the constancy of the corresponding fluxes, which yields

$$n_+u_+ = n_-u_-,$$

$$n_+[(m_1+m_2)u_+^2 + 2T_+] = n_-[(m_1+m_2)u_-^2],$$

$$n_+[(m_1+m_2)u_+^3 + 6u_+T_+] = n_-[(m_1+m_2)u_-^3]. \tag{8}$$

These are the Rankine-Hugoniot conditions, which relate the downstream and upstream values of the flow fields in the mixture [1]. Solving this system for the downstream asymptotic flow fields one finds [31]

$$n_+ = 2n_-, \quad u_+ = \frac{u_-}{2}, \quad T_+ = \frac{1}{8}(m_1+m_2)u_-^2. \tag{9}$$

Therefore, the downstream asymptotic density (velocity) is twice (half) the upstream one for $r\to\infty$. It must be noticed that these results come from the conservation laws characterizing the two-component fluid, and have nothing to do with the hydrodynamic behavior of the mixture. In this way it is not strange that even in nonhydrodynamic cases, as the equal mass version of our one-dimensional gas [28], the results [Eq. (9)] hold.

The case of a infinitely strong shock has been studied in detail for mono-component gases in dimensions larger than one [24,26]. Extending a hypothesis by H. Grad [24], we suggest here that the problem of a shock wave in our 1D mixture is in general well defined in the limit $r\to\infty$, and that in this case the distribution functions f_i can be decomposed into a singular part ($\hat{f}_i$) proportional to a Dirac δ-function on the upstream velocity u_-, and a regular part $(\tilde{f}_i)$ smoother than the former. This is because for $r\to\infty$, particles in the upstream region exhibit a well-defined fixed thermal velocity when measured on the downstream velocity scale. Hence,

$$f_i=\hat{f}_i+\tilde{f}_i, \quad \text{with} \quad \hat{f}_i(x,v)=\hat{n}_i(x)\delta(v-u_-). \tag{10}$$

The singular particle densities $\hat{n}_i(x)$ control how important the singular component is at a given coordinate x. In particular, it is evident that $\hat{n}_i(x)\to n_-$ as $x\to-\infty$, and $\hat{n}_i(x)\to 0$ as $x\to+\infty$. Introducing the above decomposition (10) into Eqs. (1) and (2), we may split the original Boltzmann equations in two different sets, attending to the singular or regular character of the terms

$$v\frac{d\hat{f}_i}{dx}+\hat{f}_i\nu(\tilde{f}_j)=\mathcal{Q}_i(\hat{f}_i,\hat{f}_j)-\hat{f}_i\nu(\hat{f}_j), \tag{11}$$

$$v\frac{d\tilde{f}_i}{dx}-\mathcal{Q}_i(\tilde{f}_i,\hat{f}_j)-\mathcal{Q}_i(\hat{f}_i,\tilde{f}_j)+\tilde{f}_i\nu(\hat{f}_j)=\mathcal{Q}_i(\tilde{f}_i,\tilde{f}_j)-\tilde{f}_i\nu(\tilde{f}_j), \tag{12}$$

with $i=1,2$. Equation (12) for the regular component $\tilde{f}_i$ looks more complicated than the original Boltzmann equations (1) and (2). However, as an advantage, it lacks the singular behavior, characterizing for $r\to\infty$ the whole distribution f_i. This allows us to perform a simple local Maxwellian approximation for $\tilde{f}_i$ that yields meaningful results. In particular, we now assume

$$\tilde{f}_i(x,v)=\tilde{n}_i(x)\sqrt{\frac{m_i}{2\pi\tilde{T}_i(x)}}\exp\left[-\frac{m_i[v-\tilde{u}(x)]^2}{2\tilde{T}_i(x)}\right]. \tag{13}$$

Here, $\tilde{n}_i(x)$, $\tilde{u}(x)$, and $\tilde{T}_i(x)$ are the number density, velocity, and temperature respectively, associated with $\tilde{f}_i$. Now $\tilde{n}_i(x)\to 0$ as $x\to-\infty$ and $\tilde{n}_i(x)\to n_+$ as $x\to+\infty$. We have also assumed at this point that the regular flow velocity $\tilde{u}(x)$ does not depend on particle species. This assumption seems natural given the one-dimensional character of the system, which forces neighboring particles to move coherently on average. Therefore, the problem of the shock wave structure reduces to computing the spatial dependence of seven different flow fields; namely, $\hat{n}_i(x)$, $\tilde{n}_i(x)$, $\tilde{T}_i(x)$, and $\tilde{u}(x)$, $i=1,2$.

It is important to notice that the Maxwellian approximation (13) is not a local thermodynamic equilibrium hypothesis, since it affects only the regular component $\tilde{f}_i(x,v)$ of the distribution function. The singular, delta-like component $\hat{f}_i(x,v)$ accounts for the most important nonequilibrium effects. However, it is natural to question the validity of (13) for the present strong nonequilibrium problem. This approximation is just the zeroth-order term in a formal expansion of $\tilde{f}_i(x,v)$ around local Maxwellian behavior, in the spirit of Sonine polynomials expansions, Gram-Charlier and Edgeworth series, etc. [32–34]. One would expect that higher-order terms in this expansion could be relevant near the shock layer. In fact, such slight deviations have been observed in monocomponent gases in higher dimensions [26]. However, these small corrections have negligible effects on the shock hydrodynamic profiles [26], and therefore are not important for our discussion here.

We may use (10) and (13) to compute the local hydrodynamic currents. Let $J_{i,n}(x)$, $J_{i,v}(x)$ and $J_{i,e}(x)$ be the particle, momentum, and energy fluxes of species i at position x, respectively. They can be written as

$$J_{i,n}(x)\equiv\int_{-\infty}^{+\infty}dv\; vf_i(x,v)=\tilde{n}_i\tilde{u}+\hat{n}_iu_-, \tag{14}$$

$$J_{i,v}(x)\equiv\int_{-\infty}^{+\infty}dv\; m_iv^2f_i(x,v)=m_i(\tilde{n}_i\tilde{u}^2+\hat{n}_iu_-^2)+\tilde{n}_i\tilde{T}_i, \tag{15}$$

$$J_{i,e}(x)\equiv\int_{-\infty}^{+\infty}dv\; m_iv^3f_i(x,v)=m_i(\tilde{n}_i\tilde{u}^3+\hat{n}_iu_-^3)+3\tilde{u}\tilde{n}_i\tilde{T}_i, \tag{16}$$

(A trivial factor $\frac{1}{2}$ has been omitted in the definition of the energy flux for convenience). Given the constancy of the total fluxes along the system, we now write the Rankine-Hugoniot conditions as

$$\tilde{n}_1\tilde{u}+\hat{n}_1u_-=n_-u_-, \tag{17}$$

$$\tilde{n}_2\tilde{u}+\hat{n}_2u_-=n_-u_-, \tag{18}$$

$$m_1(\tilde{n}_1\tilde{u}^2+\hat{n}_1u_-^2)+m_2(\tilde{n}_2\tilde{u}^2+\hat{n}_2u_-^2)+\tilde{p}_1+\tilde{p}_2=n_-(m_1+m_2)u_-^2, \tag{19}$$

$$\begin{aligned}m_1(\tilde{n}_1\tilde{u}^3+\hat{n}_1u_-^3)+m_2(\tilde{n}_2\tilde{u}^3+\hat{n}_2u_-^3)+3\tilde{u}(\tilde{p}_1+\tilde{p}_2)\\=n_-(m_1+m_2)u_-^3,\end{aligned} \tag{20}$$

where $\tilde{p}_i=\tilde{n}_i\tilde{T}_i$ is the pressure of the regular component $\tilde{f}_i$. Defining $\tilde{M}\equiv m_1\tilde{n}_1+m_2\tilde{n}_2$, $\hat{M}\equiv m_1\hat{n}_1+m_2\hat{n}_2$, $M_-\equiv(m_1+m_2)n_-$, and $\tilde{P}\equiv\tilde{p}_1+\tilde{p}_2$, we obtain

$$\tilde{M}\tilde{u}=\hat{\Delta}u_-, \quad \tilde{M}\tilde{u}^2+\tilde{P}=\hat{\Delta}u_-^2, \quad \tilde{M}\tilde{u}^3+3\tilde{u}\tilde{P}=\hat{\Delta}u_-^3, \tag{21}$$

where $\hat{\Delta}\equiv M_--\hat{M}$. Using the first relation in the second equation, one has $\tilde{P}=\hat{\Delta}u_-(u_--\tilde{u})$, and inserting this expression into the third equation yields (after division by $\hat{\Delta}u_-$) $2\tilde{u}-3u_-\tilde{u}+u_-^2=0$. This equation has solution $\tilde{u}=u_-/2$ (the second root, $\tilde{u}=u_-$, is trivial and can be neglected as incompatible with the boundary condition at $+\infty$). Therefore, the regular flow velocity is constant along the system, and equal to its asymptotic value at $+\infty$, u_+. Using this in Eqs. (17) and (18), one has

$$\tilde{n}_i(x)=2[n_--\hat{n}_i(x)], \quad i=1,2, \tag{22}$$

$$\tilde{u}(x) = \frac{1}{2}u_{-}. \tag{23}$$

Combination of these results with $\tilde{P}=\hat{\Delta}u_{-}(u_{-}-\tilde{u})$ yields a relation for the regular pressures; namely,

$$\tilde{p}_1 + \tilde{p}_2 = \frac{u_{-}^2}{4}(m_1\tilde{n}_1 + m_2\tilde{n}_2). \tag{24}$$

These manipulations are intended to express all remaining flow fields in terms of the singular particle densities $\hat{n}_i(x)$. Equations for these singular densities can be derived integrating with respect to v [Eq. (11)] for the singular component $\hat{f}_i$ [35]. This yields

$$u_{-}\frac{d\hat{n}_i(x)}{dx} = 2\alpha_j(x)\hat{n}_i(x)[\hat{n}_j(x) - n_{-}], \tag{25}$$

where

$$\alpha_i(x) \equiv \frac{u_{-}}{2}\,\mathrm{erf}\left[\sqrt{\frac{m_i}{2\tilde{T}_i(x)}}\frac{u_{-}}{2}\right] + \sqrt{\frac{2\tilde{T}_i(x)}{\pi m_i}}\exp\left[-\frac{m_i u_{-}^2}{8\tilde{T}_i(x)}\right], \tag{26}$$

and where we have used results (22) and (23). To completely specify the flow fields, we need another expression relating the regular pressures $\tilde{p}_i$ to the other fields. This relation can be derived studying the momentum and energy transfer from species i to species j. Multiplying Eq. (1) by $m_i v$ (momentum transfer) or $m_i v^2$ (energy transfer) and integrating over v, we arrive at differential equations for $J_{i,v}(x)$ and $J_{i,e}(x)$ of the form

$$\frac{dJ_{i,v}}{dx} = \Pi_i(x), \tag{27}$$

$$\frac{dJ_{i,e}}{dx} = \Xi_i(x), \tag{28}$$

where the fluxes are defined in Eqs. (15) and (16), and

$$\Pi_i(x) \equiv \int_{-\infty}^{+\infty} dv\; m_i v[\mathcal{Q}_i(f_i,f_j) - f_i\nu(f_j)], \tag{29}$$

$$\Xi_i(x) \equiv \int_{-\infty}^{+\infty} dv\; m_i v^2[\mathcal{Q}_i(f_i,f_j) - f_i\nu(f_j)]. \tag{30}$$

Since the total momentum flux, $J_{1,v}(x)+J_{2,v}(x)$, and total energy flux, $J_{1,e}(x)+J_{2,e}(x)$, are constants along the line (Rankine-Hugoniot conditions), the above differential equations (27) and (28) express the transfer of momentum and energy from species i to species j at a given point x. Using the expressions for $J_{i,v}(x)$ and $J_{i,e}(x)$ in (15) and (16), it is easy to show that $3\tilde{u}J_{i,v}(x)-J_{i,e}(x)=\frac{1}{2}m_i n_{-}u_{-}^3=$constant, and therefore,

$$3\tilde{u}\Pi_i(x) - \Xi_i(x) = 0. \tag{31}$$

This last equation will give us the desired extra relation for the regular pressures. In general, the integrals in (29) and (30) cannot be performed due to the velocity-dependent collision kernel $|v-w|$ appearing in the definition of $\mathcal{Q}_i$ and ν [see (3) and (4)]. In order to continue our derivation, we now approximate this kernel by a generic velocity-independent kernel $\sigma(x)$, much in the spirit of Maxwell molecules [29].

Using this assumption, we can solve the above integrals, obtaining

$$\Pi_i(x) = \frac{2m_i m_j}{m_i + m_j}n_{-}u_{-}\sigma(x)(N_i - N_j), \tag{32}$$

$$\Xi_i(x) = \frac{m_i m_j}{(m_i + m_j)^2}\sigma(x)\{u_{-}^2[(m_i + 2m_j)\tilde{n}_i\hat{n}_j - (m_j + 2m_i)\hat{n}_i\tilde{n}_j] - 4[N_j\tilde{p}_i - N_i\tilde{p}_j]\}, \tag{33}$$

where we have defined the species total number density, $N_i(x)\equiv\tilde{n}_i(x)+\hat{n}_i(x)=2n_{-}-\hat{n}_i(x)$, $i=1,2$. Within this approximation, Eq. (31) reduces to

$$N_j\tilde{p}_i - N_i\tilde{p}_j = \frac{u_{-}}{8}(m_j - m_i)(\tilde{n}_i\hat{n}_j + \hat{n}_i\tilde{n}_j), \tag{34}$$

which is the second relation between the regular pressures we were looking for. Together with (24), this yields

$$\tilde{p}_i = \frac{u_{-}^2[(m_j - m_i)(\tilde{n}_i\hat{n}_j + \hat{n}_i\tilde{n}_j) + 2\tilde{M}N_i]}{8(N_i + N_j)}, \tag{35}$$

where we have used the previous definition $\tilde{M}\equiv m_i\tilde{n}_i+m_j\tilde{n}_j$. This result, based on the Maxwell velocity kernel approximation, gives predictions for the regular pressures that are very close ($\forall\ x$) to the results obtained from the solution of Eq. (31) based on the numerical evaluation of integrals (29) and (30), thus validating our approximation. The reason behind this good agreement is that Eq. (34) does not depend on the collision kernel $\sigma(x)$ chosen for the Maxwell-like approximation: the same equation is found for any kernel $\sigma(x)$ one may think of, and in particular for the (unknown) optimal kernel that better approximates the real velocity-dependent kernel.

Recalling that $\tilde{n}_i=2(n_{-}-\hat{n}_i)$ and $\tilde{u}=\frac{1}{2}u_{-}$, Eqs. (35) express the regular pressures $\tilde{p}_i=\tilde{n}_i\tilde{T}_i$, and hence the regular temperatures, in terms of the singular densities $\hat{n}_i$. Therefore, the problem of the shock wave reduces to solving the coupled, strongly nonlinear differential equation (25) for $\hat{n}_i(x)$, $i=1,2$, since all other nonconstant flow fields, $\tilde{n}_i$ and $\tilde{T}_i$, with $i=1,2$, can be written in terms of $\hat{n}_i$.

III. RESULTS

The strong nonlinearities present in Eq. (25) prevent any full analytical solution to the shock wave problem, so that numerical integration must be used instead. This procedure yields the singular densities $\hat{n}_i(x)$, from which all hydrodynamic flow fields follow. We are particularly interested here in the total number density $N(x)$, flow velocity $u(x)$, and temperature $T(x)$, and their particularization to each species [$N_i(x)$, $u_i(x)$, and $T_i(x)$, $i=1,2$, respectively]. The total num-

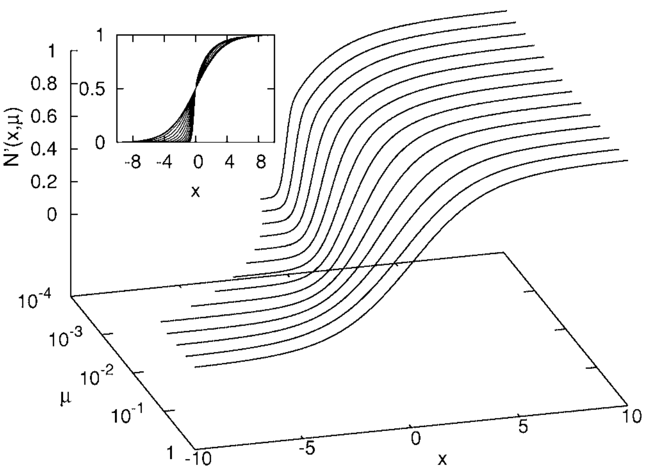

FIG. 1. Total density profiles (normalized) as a function of mass ratio μ. Notice the logarithmic scale in the μ-axis. The inset shows the same profiles in a 2D plot for better comparison.

ber density is defined as $N(x) \equiv N_1(x) + N_2(x)$, where $N_i(x) = \tilde{n}_i(x) + \hat{n}_i(x)$ has been defined above. The total flow velocity and temperature fields are defined, respectively, as $u(x) \equiv [\Sigma_i m_i N_i(x)]^{-1} \Sigma_i m_i N_i(x) u_i(x)$ and $T(x) \equiv N(x)^{-1} \Sigma_i N_i(x) T_i(x)$ [22], where

$$u_i \equiv N_i^{-1} \int_{-\infty}^{+\infty} dv \, v f_i(x,v) = \frac{n_- u_-}{N_i},$$

$$T_i \equiv N_i^{-1} \int_{-\infty}^{+\infty} dv \, m_i [v - u(x)]^2 f_i(x,v)$$

$$= \frac{\tilde{n}_i \tilde{T}_i + m_i \left[\tilde{n}_i \left(\frac{1}{2} u_- - u \right)^2 + \hat{n}_i (u_- - u)^2 \right]}{N_i}.$$

For a generic hydrodynamic flow field $\phi(x)$, we now define an associated normalized field as $\phi'(x) = (\phi(x) - \phi_-)/(\phi_+ - \phi_-)$, where $\phi_\pm = \phi(x \to \pm\infty)$. This allows us to compare shock profiles for different mass ratios $\mu \equiv m_1/m_2 \in (0,1)$. In addition, we define the normalized *excess* flow fields as $\delta\phi'(x) \equiv \phi_2'(x) - \phi_1'(x)$ to study the species dependence of the profiles. Our results for $N'(x)$, $u'(x)$, and $T'(x)$ are given in Figs. 1, 3, and 5, respectively, while the excess fields $\delta N'(x)$, $\delta u'(x)$, and $\delta T'(x)$ are depicted in Figs. 2, 4, and 6. It should be noted that we set the coordinate origin $x=0$ so that $N'(x=0) = \frac{1}{2}$.

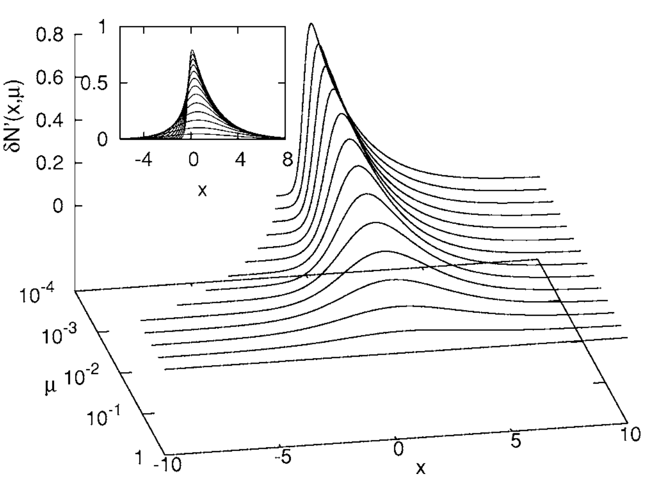

FIG. 2. Excess density profiles (normalized).

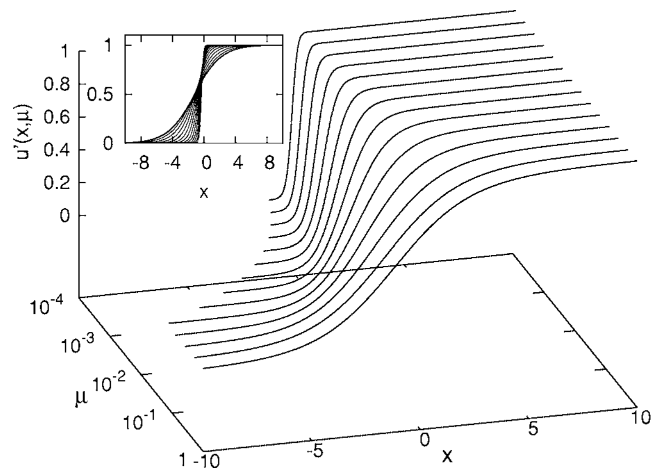

FIG. 3. Flow velocity profiles (normalized).

A general observation is that all the profiles become steeper, and the excess fields become more localized and peaked around $x=0$, as μ decreases. However, there are fundamental differences for the different hydrodynamic quantities. The density flow field $N'(x)$ converges toward a limiting shape as $\mu \to 0$, characterized by a sudden increase of density from $N'(x \to 0_-) = 0$ to $N'(x \to 0_+) = \frac{1}{2}$, followed by a much slower relaxation toward the asymptotic value $N'(x \to +\infty) = 1$ (see Fig. 1). On the other hand, the flow velocity profile $u(x)$ converges toward a step-like function localized at $x=0$ (Fig. 3), while the temperature field (Fig. 5) exhibits an overshoot which sharpens and increases as $\mu \to 0$. In addition, all profiles are markedly asymmetrical. Figure 7 exhibits all fields for several mass ratios.

The excess profiles contain the information about the relative local distribution of the hydrodynamic fields between

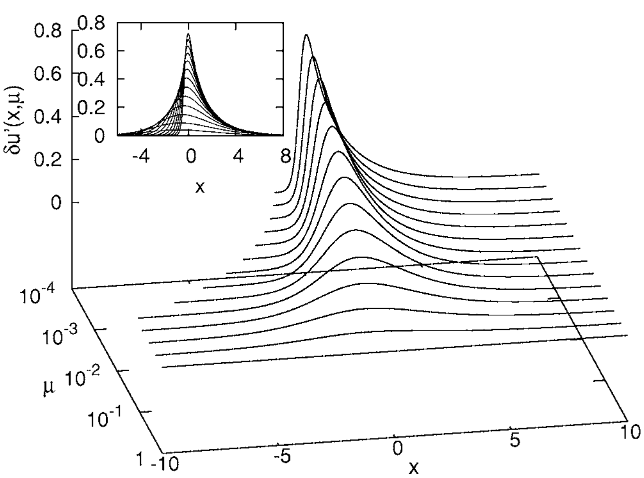

FIG. 4. Excess flow velocity profiles (normalized).

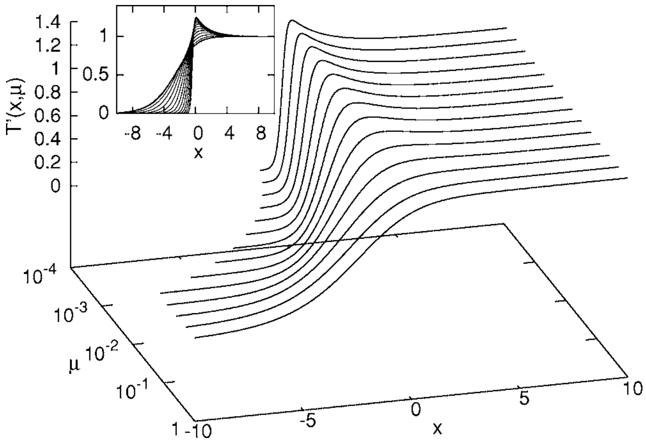

FIG. 5. Temperature profiles (normalized).

the species. In particular, $\delta N'(x)$ shows that the number density of heavy particles (type 2) around the shock layer is larger than that of light particles (type 1) (see Fig. 2). This excess concentration of heavy particles around the shock is asymmetric, with most excess heavy particles lagging behind the shock, and it increases as $\mu \to 0$. On the other hand, the flow velocity $u_1(x)$ of light particles around the shock is larger than the velocity of heavy particles [see Fig. 4], the difference increasing with decreasing μ [notice here that $\delta u'(x) > 0$ involves $u_1(x) > u_2(x)$]. Finally, the excess temperature field exhibits an interesting behavior (see Figs. 6 and 7). First, $\delta T'(x)$ is mostly negative near the shock, so heavy particles are cooler than light particles around the shock, despite the former are denser than the latter around $x=0$. In more detail, $\delta T'(x)$ exhibits an oscillation around $x=0$, meaning that heavy particles are much colder than light particles *behind* the shock layer (the cooler the smaller μ is), while the situation is reversed *in front* of the shock, where heavy particles are now more energetic than light ones (see Fig. 6).

To better understand some of these observations, we can analyze the asymptotic behavior of Eqs. (25). First, we study how the downstream binary fluid goes toward equilibrium by

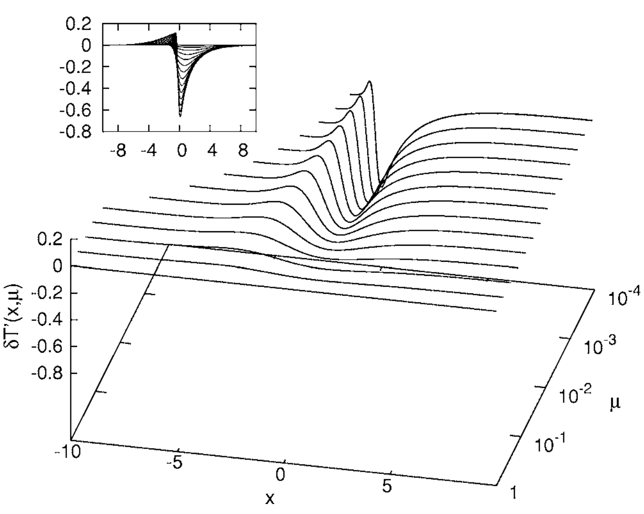

FIG. 6. Excess temperature profiles (normalized).

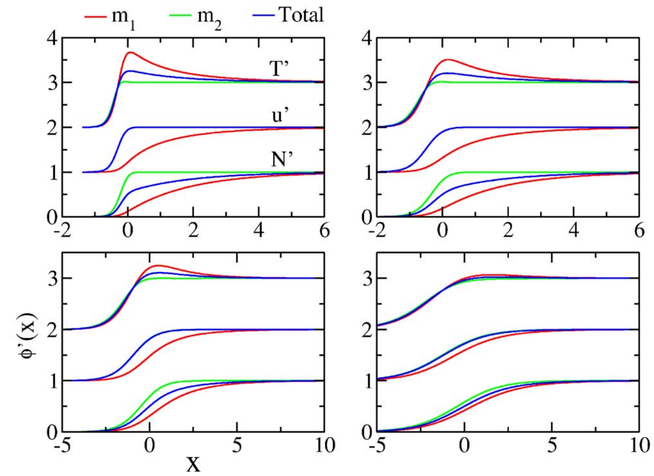

FIG. 7. (Color online) Density, velocity, and temperature profiles for each species and the mixture. From left to right and top to bottom, μ=0.000 125, 0.001, 0.016, 0.128. Velocity (temperature) profiles have been shifted one (two) units in the vertical axis for visual convenience.

letting $x \gg 0$. In this case, the singular densities are very small $[\hat{n}_i(x \gg 0) \ll 1]$, so that we can linearize Eqs. (25), obtaining a simple decoupled system of differential equations

$$u_- \frac{d\hat{n}_i(x)}{dx} = -2\alpha_j(+\infty) n_- \hat{n}_i(x), \tag{36}$$

with $i=1,2$, and where

$$\alpha_i(+\infty) = \frac{u_-}{2}\left[\operatorname{erf}\left(\sqrt{\frac{m_i}{m_1+m_2}}\right) + \sqrt{\frac{m_1+m_2}{\pi m_i}} \exp\left(-\frac{m_i}{m_1+m_2}\right)\right] \tag{37}$$

is the limit of the amplitudes (26) as $x \to +\infty$. Therefore, we find $\hat{n}_i(x) \sim \exp[-x/\lambda_j]$ in this limit, with $\lambda_j = u_-/[2n_-\alpha_j(+\infty)]$, so the downstream binary fluid reaches equilibrium exponentially fast, as expected from the uncorrelated nature of the Boltzmann equation [21–23]. This equilibration process is characterized however by two different typical scales: λ_1 controls how heavy particles (type 2) relax asymptotically, while λ_2 controls the behavior of light particles (type 1). The μ-dependence of both typical scales is depicted in Fig. 8. Here we see that $\lambda_2 > \lambda_1 \forall\ \mu \in (0,1)$. In fact, λ_2 converges to a constant as $\mu \to 0$, while λ_1 goes asymptotically to 0 as $\mu^{1/2}$ [see Eq. (37)]. Therefore, a separation of scales emerges for very small mass ratios μ, with both fast and slow evolution scales controlling the fluid relaxation. All the macroscopic hydrodynamic fields $\phi(x)$ relax asymptotically as $\exp[-x/\lambda_2]$, following the slowest relaxation scale associated with light particles, except for the number density for heavy particles, which relax much faster, as $\exp[-x/\lambda_1]$.

In the opposite limit, $\mu \to 1$, a singularity emerges. In fact, the Boltzmann equation does not yield any useful information for $\mu=1$ in one dimension: the gain and loss terms in the collision operator are equal in this case, so that the collision term in the Boltzmann equation is zero [see right-hand side

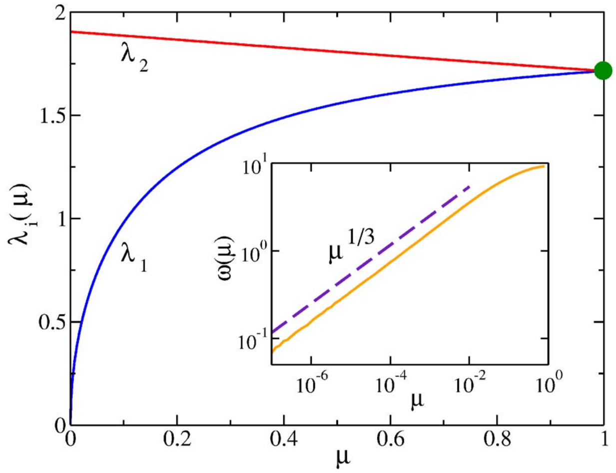

FIG. 8. (Color online) Mass ratio dependence of the typical scales λ_i controlling the exponential relaxation of the downstream binary fluid toward equilibrium. Notice that λ_1 scales as $\mu^{1/2}$ for small μ. The solid dot signals the singular limit $\mu=1$, for which both typical scales formally diverge. Inset: Mass ratio dependence of the shock width ω in log-log scale. The width decreases as $\omega \sim \mu^{1/3}$ for $\mu \to 0$.

of Eqs. (1) and (2)]. That is, collisions do not change the velocity distributions $f_i(x,v)$ in this limit, as expected from the fact that equal-mass particles exchange their velocities upon collision in 1D. Therefore there is no relaxation of hydrodynamic fields for $\mu=1$, and the relaxation scales λ_i are not defined. Alternatively, this can be interpreted as a divergence of both λ_i. However, this is a singular behavior that emerges only for $\mu=1$. As soon as $\mu<1$, normal behavior is recovered. In particular, for μ slightly smaller than 1, one expects both typical scales to be almost equal, as observed in Fig. 8.

The separation of scales described above for $\mu \to 0$ does not only emerge for $x \to +\infty$, but characterizes the profiles $\forall\ x$. In fact, the amplitudes $\alpha_i(x)$ [see eqs. (26)], are such that $\alpha_1(x) \gg \alpha_2(x) \forall\ x$ as $\mu \to 0$. Hence, in this limit the singular density $\hat{n}_2(x)$ changes at a much faster rate than $\hat{n}_1(x)$ does (see Eqs. (25)), so that we can consider $\hat{n}_1(x)$ as a constant in the scale in which $\hat{n}_2(x)$ evolves. This effectively decouples again the differential equations (25) (though they are still highly nonlinear), giving rise to a multiscale relaxation process. (i) In a first step, heavy particles very quickly relax toward their equilibrium downstream asymptotic state while light particles remain close to the upstream state. (ii) This is followed by a relatively much slower relaxation of light particles toward equilibrium. A good illustration of this process can be found in the top-left panel in Fig. 7. This two-scale relaxation mechanism for $\mu \to 0$ explains the limiting shape described above for $N'(x)$ (see Fig. 1), as well as the the positive excess density $\delta N'(x)$ in Fig. 2. In addition, it also explains the step-like limiting profile for the flow velocity: $u(x)$ is the weighted average of the species flow velocities $u_i(x)$, the weigh being proportional to the species mass, so for $\mu \to 0$, $u(x)$ coincides with $u_2(x)$, which is controlled by the fastest relaxation scale.

It also seems interesting to characterize the region where the fluid is far from equilibrium. A *canonical* measure of the scale or typical size associated with this region is given by the shock width ω. The shock width is usually defined as the inverse of the maximum density profile derivative, $\omega(\mu) \equiv (dN/dx)^{-1}_{\max}$ [1]. It can be also defined as the standard deviation of the (peaked) *distribution* $AN'(x)[1-N'(x)]$, with A a suitable normalization constant. Both definitions give equivalent results. The inset to Fig. 8 shows our results for $\omega(\mu)$. The shock width decreases as the mass ratio decreases, scaling as $\omega(\mu) \sim \mu^{1/3}$ for $\mu \to 0$ [36]. Therefore, nonequilibrium effects are more localized around $x=0$ for smaller μ. However, it is remarkable that despite the shock wave gets steeper (ω decreases) as μ decreases, the typical scale characterizing relaxation toward equilibrium, λ_2, increases with μ. Hence, although the strong nonequilibrium region is reduced as $\mu \to 0$, the consequent fluid evolution to equilibrium slows down.

IV. CONCLUSIONS

In this paper we have studied the response of a one-dimensional binary fluid to a strong shock wave propagating into it, on the basis of the Boltzmann equation. This excitation drives the system far from equilibrium, therefore allowing us to investigate the structure of the fluid under nonequilibrium conditions and how equilibrium is regained asymptotically.

Extending to fluid mixtures an elegant method by H. Grad [24,26], we have obtained the shock hydrodynamic profiles characterizing the transition between the two different asymptotic equilibrium states. In particular, we determine the flow fields as a function of the mixture mass ratio $\mu = m_1/m_2 \in (0,1)$. We find in general that all profiles sharpen as $\mu \to 0$. The particle number density field converges in this limit to an asymptotic shape characterized by a sudden step-like increase followed by a much slower relaxation to equilibrium. The flow velocity profile converges in turn to a step-like function, while the temperature field exhibits a characteristic overshoot which increases with decreasing μ. In addition, the density (velocity) of heavy particles *behind* the shock is larger (smaller) than that of light particles, the differences increasing as $\mu \to 0$. On the other hand, heavy particles are much cooler than light particles right behind the shock, while the reverse situation holds in front of the shock, where heavy particles are now slightly more energetic than light ones.

In order to understand these results, we have performed an asymptotic analysis of our equations. This reveals the emergence of two very different typical length scales controlling relaxation as $\mu \to 0$. In this limit, the fluid evolves toward equilibrium in twos steps. (i) First, heavy particles quickly relax toward their asymptotic downstream equilibrium state, while light particles remain close to the upstream state. (ii) At a much slower pace, light particles come to equilibrium. In this way, light particles ultimately control the fluid's global equilibration. Far behind the shock layer, the hydrodynamic fields relax exponentially. Here the multiscale relaxation mechanism is also apparent, with two typical exponential scales λ_i, $i=1,2$. In particular, λ_1, associated with heavy particles, goes to zero as $\mu^{1/2}$, while λ_2, which controls the global relaxation to equilibrium, increases as $\mu \rightarrow 0$, converging to a constant. In addition, the size of the strong nonequilibrium region associated with the shock layer, as measured by the shock width $\omega(\mu)$, decreases as $\omega(\mu) \sim \mu^{1/3}$ for $\mu \rightarrow 0$. Therefore, the fluid's strong nonequilibrium behavior gets more localized around $x=0$ as μ decreases, despite its asymptotic relaxation to equilibrium, as given by λ_2, slows down with decreasing μ.

These results are specially interesting at the light of recent numerical studies of similar 1D binary fluids [12,13,15,18,20,37,38]. In particular, simulations show that whenever the 1D binary fluid is perturbed away from equilibrium, the consequent relaxation happens in such a way that light particles always tend to absorb more energy than heavy ones, as predicted here. In addition, light particles are observed to equilibrate more slowly, therefore controlling the system global relaxation. This supports the presence of two different relaxation scales for $\mu \rightarrow 0$, validating our theoretical results.

The success of our Boltzmann equation approach to describe some of the structural and relaxational anomalies observed in the 1D diatomic fluid would suggest extending the present approach to understand its anomalous transport properties (see Sec. I) [12–18]. Unfortunately, this is not possible. Anomalous transport in 1D is a direct consequence of the long-time power-law tails characterizing the decay of correlation functions in the fluid. The microscopic origin of these tails is associated to dynamically correlated sequences of collisions among fluid molecules, which are not described by the Boltzmann equation [39]. That is, the main hypothesis on which the Boltzmann equation is based; namely, the *molecular chaos* hypothesis [21–23], breaks correlations present in the fluid that are responsible of the power-law tails.

The strong correlations emerging in 1D fluids, and its role in the shock wave problem, are interesting issues that deserve attention [37,40]. Further work in this direction, taking into account these correlations in generalized kinetic theories, would be highly desirable to better understand the nonequilibrium behavior of simple one-dimensional systems.

ACKNOWLEDGMENTS

The author thanks P.L. Garrido and P.L. Krapivsky for useful comments and discussions, as well as the Spanish MEC for financial support.

[1] G. B. Whitham, *Linear and Nonlinear Waves* (Wiley-Interscience, New York, 1999).
[2] S. Lepri, R. Livi, and A. Politi, Phys. Rev. Lett. **78**, 1896 (1997); Phys. Rep. **377**, 1 (2003).
[3] *Nonequilibrium Statistical Mechanics in One Dimension*, edited by V. Privman (Cambridge University Press, Cambridge, 1997).
[4] J. Hone, M. Whitney, C. Piskoti, and A. Zettl, Phys. Rev. B **59**, R2514 (1999); P. Kim, L. Shi, A. Majumdar, and P. L. McEuen, Phys. Rev. Lett. **87**, 215502 (2001).
[5] D. T. Morelli, J. Heremans, M. Sakamoto, and C. Uher, Phys. Rev. Lett. **57**, 869 (1986); A. Smontara, J. C. Lasjaunias, and R. Maynard, *ibid.* **77**, 5397 (1996).
[6] A. V. Sologubenko, K. Giannó, H. R. Ott, A. Vietkine, and A. Revcolevschi, Phys. Rev. B **64**, 054412 (2001).
[7] H. Forsman and P. Anderson, J. Chem. Phys. **80**, 2804 (1984).
[8] L. G. C. Rego and G. Kirczenow, Phys. Rev. Lett. **81**, 232 (1998); D. M. Leitner and P. G. Wolynes, Phys. Rev. E **61**, 2902 (2000).
[9] V. Kukla *et al.*, Science **272**, 702 (1996); K. Hahn, J. Kärger, and V. Kukla, Phys. Rev. Lett. **76**, 2762 (1996).
[10] M. Porter, Bull. Am. Phys. Soc. **50**, 1047 (2005).
[11] T. E. Harris, J. Appl. Probab. **2**, 323 (1965); D. G. Levitt, Phys. Rev. A **8**, 3050 (1973); Q.-H. Wei, C. Bechinger, and P. Leiderer, Science **287**, 625 (2000); B. Cui, H. Diamant, and B. Lin, Phys. Rev. Lett. **89**, 188302 (2002); C. Lutz, M. Kollmann, and C. Bechinger, *ibid.* **93**, 026001 (2004).
[12] P. L. Garrido, P. I. Hurtado, and B. Nadrowski, Phys. Rev. Lett. **86**, 5486 (2001).
[13] P. L. Garrido and P. I. Hurtado, Phys. Rev. Lett. **88**, 249402 (2002); A. Dhar, *ibid.* **88**, 249401 (2002); P. L. Garrido and P. I. Hurtado, *ibid.* **89**, 079402 (2002); H. Li, Y. Wang, and H. Zhao, *ibid.* **89**, 079401 (2002).
[14] O. Narayan and S. Ramaswamy, Phys. Rev. Lett. **89**, 200601 (2002).
[15] P. Grassberger, W. Nadler, and L. Yang, Phys. Rev. Lett. **89**, 180601 (2002); P. Cipriani, S. Denisov, and A. Politi, Phys. Rev. Lett. **94**, 244301 (2005).
[16] J.-S. Wang and B. Li, Phys. Rev. Lett. **92**, 074302 (2004).
[17] A. Pereverzev, Phys. Rev. E **68**, 056124 (2003).
[18] A. Dhar, Phys. Rev. Lett. **86**, 3554 (2001); A. V. Savin, G. P. Tsironis, and A. V. Zolotaryuk, *ibid.* **88**, 154301 (2002); G. Casati and T. Prosen, Phys. Rev. E **67**, 015203(R) (2003).
[19] B. Li, G. Casati, J. Wang, and T. Prosen, Phys. Rev. Lett. **92**, 254301 (2004).
[20] A. Kato and D. Jou, Phys. Rev. E **64**, 052201 (2001).
[21] P. Résibois and M. de Leener, *Classical Kinetic Theory of Fluids* (John Wiley & Sons, New York, 1977).
[22] S. R. de Groot and P. Mazur, *Nonequilibrium Thermodynamics* (Dover, New York, 1984).
[23] S. Harris, *An Introduction to the Theory of the Boltzmann Equation* (Dover, New York, 2004).
[24] H. Grad, in *Transport Theory*, edited by R. Bellman, G. Birkhoff, and I. Abu-Shumays, (American Mathematical Society, Providence, R. I., 1969), pp. 269–308.
[25] H. Mott-Smith, Phys. Rev. **82**, 885 (1951).
[26] C. Cercignani, A. Frezzotti, and P. Grosfils, Phys. Fluids **11**, 2757 (1999).
[27] D. W. Jepsen, J. Math. Phys. **6**, 405 (1965).
[28] For $m_1 = m_2$, the fluid studied in this paper reduces to an ideal one-dimensional gas of noninteracting particles. This system is not ergodic, and lacks any relaxation mechanism in velocity space capable of driving the system toward local thermodynamic equilibrium.

[29] R. Dickman, J. Stat. Phys. **41**, 607 (1985); O. J. Eder and M. Posch, Phys. Rev. A **34**, 2283 (1986).

[30] Notice that the asymptotic number densities $n_{\pm}$ do not depend on the species, since we are interested here on a 1D binary fluid with *equal* concentrations of light and heavy particles.

[31] In this process we disregard a trivial solution $u_{+}=u_{-}$ which is incompatible with the boundary condition at $+\infty$.

[32] *Handbook of Mathematical Functions with Formulas, Graphs, and Mathematical Tables*, 9th printing edited by M. Abramowitz and I. A. Stegun (Dover, New York, 1972).

[33] S. Blinnikov and R. Moessner, Astron. Astrophys., Suppl. Ser. **130**, 193 (1998).

[34] See, for instance, E. W. Weisstein, *Edgeworth Series*, from *MathWorld-A Wolfram Web Resource*, http://mathworld.wolfram.com/EdgeworthSeries.html

[35] Computing the time evolution of any moment of $\hat{f}_i$ from Eq. (11) always gives rise to the same equation for $\hat{n}_i(x)$; namely, Eq. (25).

[36] It should be noticed that, due to the separation of scales as $\mu \to 0$, $\omega(\mu)$ is given in this limit by $u_{-}/\{2\alpha_1(x)\hat{n}_1(x)[n_{-}-\hat{n}_2(x)]\}_{\max}$.

[37] Pablo I. Hurtado, cond-mat/0507689.

[38] P. I. Hurtado and S. Redner , cond-mat/0507485; cond-mat/0507651.

[39] More technically, the Boltzmann equation for hard spheres (in any dimension) is unable to predict the long-time behavior of correlation functions due to the discrete character of the collision operator spectrum. In this case the long-time behavior is determined by the smallest nonzero eigenvalue of the collision operator, and this yields an exponential decay of correlations, instead of the observed power-law [17].

[40] A. F. Andreev and A. É. Meĭerovich, Sov. Phys. JETP **37**, 829 (1973).